PDGFRα inhibition reduces myofibroblast expansion in the fibrotic rim and enhances recovery after ischemic stroke

Jil Protzmann[1], Manuel Zeitelhofer[1], Christina Stefanitsch[1], Daniel Torrente[2,a], Milena Z. Adzemovic[1,b], Kirils Matjunins[1], Stella J.I. Randel[1], Sebastian A. Lewandowski[1,b], Lars Muhl[1,c], Ulf Eriksson[1], Ingrid Nilsson[1], Enming J. Su[2], Daniel A. Lawrence[2], and Linda Fredriksson[1,*]

Author affiliations:

1 Department of Medical Biochemistry and Biophysics, Karolinska Institutet, Stockholm, Sweden

2 Department of Internal Medicine, University of Michigan Medical School, Ann Arbor, MI, USA

Current address:

[a]Patricia and John Rosenwald Laboratory of Neurobiology and Genetics, The Rockefeller University, New York, NY, USA

[b]Department of Clinical Neuroscience, Karolinska Institutet, Center for Molecular Medicine, Stockholm, Sweden;

[c]Department of Medicine Huddinge, Karolinska Institutet, Huddinge, Sweden

*Correspondence to: Linda Fredriksson

Department of Medical Biochemistry and Biophysics,

Division of Vascular Biology

Karolinska Institutet,

Biomedicum Q6D,

Solnavägen 9,

SE-171 65 Stockholm, Sweden

linda.fredriksson@ki.se

+46707396765

Running title: Fibrotic scarring in ischemic stroke

Keywords: stroke; blood-brain barrier; reactive gliosis; fibrosis; myofibroblasts

Conflict-of-interest statement

Drs. U. Eriksson, D.A. Lawrence, E.J. Su, and L. Fredriksson hold patents on modulating blood-neural barrier using PDGFR-alpha antagonist (patent numbers US8765671B2, PCT/SE2017/050183 and WO2017151043A1). U. Eriksson is a shareholder in Paracrine Therapeutics AB (Bålsta, Sweden) who provided the m6B3 anti-PDGF-CC monoclonal antibody. The other authors declare that the research was conducted in the absence of any commercial or financial relationships that could be construed as a potential conflict of interest.

Abstract

Ischemic stroke is a major cause of adult disability. Early treatment with thrombolytics and/or thrombectomy can significantly improve outcomes; however, following these acute interventions, treatment is limited to rehabilitation therapies. Thus, the identification of therapeutic strategies that can help restore brain function in the post-acute phase remains a major challenge. Here we report that genetic or pharmacologic inhibition of the PDGF-CC/PDGFRα pathway, which has previously been implicated in stroke pathology, significantly reduced myofibroblast expansion in the border of the fibrotic scar and improved outcome in a sensory-motor integration test after experimental ischemic stroke. This was supported by gene expression analyses of cerebrovascular fragments, showing upregulation of pro-fibrotic/pro-inflammatory genes, including genes of the TGFβ pathway, after ischemic stroke or intracerebroventricular injection of active PDGF-CC. Further, longitudinal intravital two-photon imaging revealed that inhibition of PDGFRα dampened the bi-phasic pattern of stroke-induced vascular leakage and enhanced vascular perfusion in the ischemic lesion. Importantly, we found efficacy of PDGFRα inhibition on functional recovery when initiated 24 hours after ischemic stroke. Our data implicate the PDGF-CC/PDGFRα pathway as a crucial mediator modulating post-stroke pathology and suggest a post-acute treatment opportunity for ischemic stroke patients targeting myofibroblast expansion to foster long-term CNS repair.

Introduction

Ischemic stroke represents a major public health challenge and is currently the second leading cause of disability and death worldwide (1). Treatment options are limited to early treatment with intravenous thrombolysis with recombinant tissue plasminogen activator (tPA) and/or mechanical thrombectomy (2). Despite these acute interventions, up to 40% of the patients will die or remain functionally dependent. More importantly, due to various contraindications, only a fraction of all ischemic stroke patients will receive these therapies. Much effort has therefore been invested in researching additional treatment options, mainly focusing on direct neuroprotection. However, due to the limited success of neuroprotective approaches, studies examining the therapeutic potential of preserving or restoring the integrity of the blood-brain barrier (BBB) have been gaining interest (3).

Damage to the BBB is an early pathological event in ischemic stroke, and the absence of a functional BBB will lead to profound disturbances in neuronal and glial signaling (4). Several molecular pathways have been reported to play important roles in disease-induced BBB damage, including our previous studies demonstrating a role for tPA-induced activation of platelet-derived growth factor receptor alpha (PDGFRα) signaling in perivascular cells in the neurovascular unit (NVU) via catalysis of the ligand platelet-derived growth factor CC (PDGF-CC) (5-11). Studies from our lab and others have shown that administering imatinib, a receptor tyrosine kinase (RTK) inhibitor of PDGFRs, ABL and c-KIT (12), significantly improves outcome after both ischemic and hemorrhagic stroke in rodents (9, 13, 14) and importantly in humans (15). The beneficial effect of

imatinib has been ascribed to its ability to reduce stroke-induced BBB leakage, but how this exactly translates to improved neurological outcome is yet unknown.

It has previously been shown that cells in the NVU act as sensors for insults to the brain and that they elicit activation of the early reactive gliosis response; in which astrocytes, NG2-glia cells (also referred to as oligodendrocyte progenitor cells, OPCs) and microglia become activated, leukocytes infiltrate and a cascade of post stroke neuropathology is initiated (16). The reactive gliosis response is an important early injury response (occurring hours to days after disease onset), which is considered to orchestrate the subsequent scar formation in the subacute/chronic phase after the insult (days to weeks after onset) (17). The CNS scar consists of an outer glial component formed by reactive glia cells and an inner fibrotic core harboring mainly fibroblasts and immune cells. Demarcation of the lesion by activated glia cells is thought to limit the spread of cellular death and confine chronic inflammation at the lesion site, thereby protecting the relatively unaffected surrounding CNS tissue. Scar formation is fundamental for injury resolution, however, it is also deleterious to functional recovery (18), as it has been shown that the glial component of the scar has inhibitory effects on CNS axonal regrowth (19).

It has been proposed that poor CNS recovery may be mechanistically similar to chronic/unresolved wounds in peripheral tissues (20). A key phase in the peripheral wound healing process is the expansion (proliferation/migration/differentiation) of contractile myofibroblasts from yet to be established progenitor cells (21). Myofibroblasts will contribute to repair by generating contractile forces enabling the

surrounding tissue to contract and close the wound. Normally, after the successful completion of repair, the myofibroblast scar will resolve, but in cases of pathology, myofibroblasts accumulate and synthesize an excessive amount of extracellular matrix (ECM) with a composition different to that of normal tissue ECM (21). It has been shown that the increased stiffness and pro-fibrotic composition of this ECM contributes to distortion of the parenchymal architecture, thus leading to compromised organ recovery and function. A master regulator of myofibroblast differentiation is transforming growth factor beta (TGFβ) that, via canonical signaling via SMAD mediators, will induce upregulation of myofibroblast characteristic markers, including alpha-smooth muscle actin (ASMA) and fibronectin (FN) (21). Interestingly, recent research has demonstrated a functional cross-talk between TGFβ and PDGFRα signaling pathways in regulating myofibroblast migration and differentiation in skeletal muscle regeneration (22) and PDGFRα has been implicated in the temporal control of fibroblast-to-myofibroblast transition in skin wound healing (23).

In the present study, we utilized a photothrombotic murine model of experimental ischemic stroke to investigate the interrelationship between stroke-induced cerebrovascular changes and CNS repair. Using longitudinal in vivo two-photon microscopy (24), we found that imatinib blocked stroke-induced vascular leakage, which coincided with preserved cellular organization in the NVU in the acute phase after ischemic stroke. Gene expression analyses of cerebrovascular fragments isolated from the ipsilateral hemisphere of imatinib-treated mice and their vehicle-treated controls identified differential expression of pathways associated with inflammation and fibrosis. Immunohistological analyses showed that imatinib dampened the acute reactive gliosis

response and subsequent myofibroblast expansion after stroke, whilst having very limited effect on the remainder of the glial scar. Assessment of a sensory-motor integration test revealed that functional benefit with imatinib treatment progressively improved over time and importantly, demonstrated efficacy of imatinib treatment also when administered in the post-acute phase after ischemic onset. Using an anti-PDGF-CC neutralizing antibody (25, 26), and genetic ablation of *Pdgfra* in glial fibrillary acidic protein $(GFAP)^+$ cells we were able to confirm that the effect of imatinib on myofibroblast expansion is mediated via activation of the PDGF-CC/PDGFRα pathway. Taken together our results suggest myofibroblast expansion as a potential post-acute target to foster CNS repair after ischemic stroke.

Results

Imatinib preserves BBB integrity and organization of the NVU in the acute phase after MCAO

TPA-mediated activation of PDGF-CC/PDGFRα signaling in the NVU during ischemic stroke in mice induces opening of the BBB and augments brain injury (9). Blocking this pathway with imatinib, a RTK inhibitor, improves outcome following ischemic stroke in both mice (9) and human patients (15). To further delineate the downstream mechanism of PDGF-CC/PDGFRα signaling in ischemic stroke, we performed vascular leakage-, gene expression- and immunofluorescent analyses in mice treated with imatinib or anti-PDGF-CC neutralizing antibody (pre-treatment if not stated otherwise), or in mice where perivascular PDGFRα had been ablated (see study outline in Supplementary Figure S1A). Utilizing intravital two-photon imaging of stroke-induced BBB breach (24), which enables longitudinal studies of vascular leakage following middle cerebral artery occlusion (MCAO) of the cortical segment of the MCA, we determined the kinetics of extraluminal cerebral leakage from the first hours post ischemia (hpi) to 7 days post ischemia (dpi) (asterisks, Figure 1A). We found that imatinib significantly reduced ischemic stroke-induced extravasation of the intravenously administered fluorescent dye FITC70 into the brain parenchyma compared to controls (Figure 1B). In accordance with previous published data (27), we observed a bi-phasic pattern of vascular leakage, with the first peak of extraluminal FITC70 occurring within hours post ischemia and the second at 3 dpi. We found that both waves were reduced by imatinib treatment. Further analysis of the first wave of MCAO-induced BBB leakage with Evans blue (EB) dye revealed that already 1 hpi the BBB was losing its integrity (Figure 1C). At 3 hpi we detected the highest

leakage, which was followed by a time-dependent decrease in EB extravasation. Imatinib treatment significantly reduced MCAO-induced EB extravasation both at 3 hpi and 24 hpi compared to vehicle-treated controls (Figure 1C). This coincided with a significantly lower number of microbleeds at 3 hpi, as detected by immunofluorescent staining for the red blood cell marker TER119, mainly around medium-to-large diameter vessels in the ischemic area of imatinib-treated mice compared to vehicle controls (Supplementary Figure S1, B-D).

It is plausible that the MCAO-increased permeability is due to a loss of endothelial tight junctions (TJ) and we therefore performed stainings with the TJ marker claudin-5 (CLDN5) at 3 hpi, a time point when extensive BBB breach was observed. Our analysis revealed no significant difference in CLDN5 immunofluorescent signal in vessels in the ischemic area between the treatment groups at 3 hpi (Supplementary Figure S1, E-H), which is in line with the current literature suggesting that the first wave of BBB breakdown in ischemic stroke is driven by increased trans-endothelial transport and not the result of increased para-cellular permeability due to TJ disassembly (28, 29). It should however be noted that it is still possible that TJ modifications such as phosphorylation, as e.g. shown for occludin (30), might affect BBB integrity despite normal expression and localization of TJ markers.

Our staining for the endothelial marker CD31 revealed that MCAO provoked a decrease in the number of vessels with a diameter >10 µm in the ischemic region of vehicle controls at 3 hpi, and that this was significantly alleviated by imatinib-treatment (Supplementary Figure S1I). It is possible that these MCAO-provoked vascular changes

are caused by vascular constriction, vascular rarefaction, collateral recruitment etc., and to test this we performed two-photon analysis of vessel diameter in endothelial cell reporter mice. This revealed a global vessel constriction (compared to their vessel diameter before ischemia) affecting all vessel types in the vascular tree 1-2 hpi (Figure 1D). Assessment of the change in vessel diameter along the arteriovenous axis showed that the arterial segments in both untreated and imatinib treated mice were most constricted. Imatinib significantly mitigated vasoconstriction in the arterial and venous segments, while the capillary diameter was unchanged (Supplementary Figure S1, J-L). Further analyses of the NVU demonstrated that imatinib treatment preserved normal levels of perivascular expression of PDGFRα as well as perivascular expression of GFAP around medium-to-large sized vessels within the ischemic area at 3 hpi (arrows) (Figure 1, E-H). Contrary, the immunoreactivity of these two markers were largely lost or scattered around vessels in the ischemic area of vehicle controls (two-headed arrows), whereas non-vascular GFAP signal appeared increased (asterisks, Figure 1F). Taken together this suggests that imatinib treatment maintains vascular health after ischemic stroke.

Imatinib regulates expression of genes associated with fibrosis and inflammation in the cerebrovasculature after MCAO

Based on these findings we isolated cerebrovascular fragments at different timepoints after MCAO from mice treated with imatinib or their vehicle controls, and performed gene expression and pathway analyses. Assessment of gene expression in the cerebrovasculature identified 121 and 85 differentially expressed transcripts at 3 hpi and

24 hpi, respectively (Supplementary Figure S2A; Supplementary Table 1 and 2), of which some of the top regulated genes were validated by qPCR analysis (Figure 2, A-C; Supplementary Figure S2, B and C). Pathway analysis revealed that functions related to fibrosis, vascular damage, inflammation as well as leukocyte adhesion were modulated by imatinib treatment (Supplementary Figure S2, D and E). Subsequent comparison to the harmonizome databank (31) confirmed these findings and revealed that approximately 30% of the imatinib-regulated transcripts were associated with fibrosis and 15% with inflammation at both 3 hpi and 24 hpi (Supplementary Figure S2, F and G). Since imatinib has shown benefit in experimental models of hemorrhagic stroke (13) and reduced the number of microbleeds (Supplementary Figure S1D), we compared our microarray data with the publicly available microarray dataset from the perihematomal area of human stroke patients (GSE24265) (32), an area associated with BBB disruption and high levels of edema formation (33). The analysis revealed high overlap and approximately half of the overlapping genes were found to be associated with fibrosis (Supplementary Figure S2, H and I; Supplementary Table 3 and 4), thus supporting that our murine analyses might be of relevance for human stroke pathology.

As the highest proportion of differentially regulated genes after imatinib treatment were associated with fibrosis and inflammation, we performed qPCR analysis on cerebrovascular fragments isolated at 3 hpi, 24 hpi and 7 dpi to analyze the expression of selected pro-fibrotic/pro-inflammatory genes. We found that MCAO induced expression of the fibrosis-associated genes *Itgax, Ccl5, Hpse, Col5a2, Fn1*, *Icam1, Il1a*, and *Mmp9* were all significantly reduced at various timepoints by imatinib treatment (Figure 2, A-H). Many of these genes, e.g. *Ccl5, Icam1*, *Il1a* and *Itgax*, have also been

associated with the inflammatory response. We further investigated the effect of imatinib treatment on the expression of genes within the PDGF-CC/PDGFRα pathway by qPCR. In accordance with our transcriptome analysis, MCAO-induced cerebrovascular expression of *Pdgfra* was significantly inhibited in imatinib-treated animals at 24 hpi compared to vehicle-treated animals (Figure 2I), whilst gene expression of *Pdgfrb* was unaffected by imatinib treatment (Figure 2J). In addition, both *Pdgfc* and *Plat* (the gene encoding for tPA), were downregulated by imatinib treatment compared to vehicle control (Figure 2, K and L).

To establish whether the PDGF-CC/PDGFRα pathway can trigger expression of fibrotic genes in the cerebrovasculature per se, active PDGF-CC protein was administered by intracerebroventricular (ICV) injection in naïve mice and cerebrovascular fragments isolated four hours later. qPCR analysis revealed that PDGF-CC injection significantly led to cerebrovascular upregulation of the fibrosis- and inflammation-associated genes *Col5a2* and *Cxcl10* (Figure 2, M and N). Both these genes were found to be downregulated following imatinib treatment in MCAO (Figure 2D; Supplementary Table 1). Interestingly, members of the TGFβ signaling pathway *(Tgfb* and *Smad3)*, known master regulators of myofibroblast differentiation (21) and key to epithelial/endothelial-to-mesenchymal transition (EMT/EndoMT) (34), were significantly upregulated after ICV injection of active PDGF-CC (Figure 2, O and P).

Imatinib attenuates the reactive gliosis response within hours after MCAO

Given the above findings, implicating PDGF-CC/PDGFRα in the fibrotic injury response, we next investigated the effect of imatinib on reactive gliosis, the immediate early injury response in the CNS know to orchestrate the formation of the fibrotic scar (17). Among the glial cells taking part in reactive gliosis are astrocytes, NG2-glia cells and microglia, which are activated/recruited to the site of insult. Since astrocytes are known to react to injury by hypertrophy and up-regulation of GFAP in the acute phase following the insult (35), we assessed astrogliosis by staining for GFAP at 3 hpi. We found increased non-vascular GFAP signal (asterisks) in the ischemic area compared to the non-ischemic surrounding tissue in vehicle-treated controls (Figure 3, A and B), which was significantly reduced in imatinib-pretreated animals (Figure 3C). The difference in non-vascular GFAP signal between treatment groups at 3 hpi was not due to a difference in the total number of astrocytes, as staining for the astrocyte-specific nuclear marker SOX9 detected no difference in the number of $SOX9^+$ nuclei in the ischemic area between vehicle- and imatinib-treated animals (Supplementary Figure S3, A-C). Further analysis of the reactive gliosis response showed that NG2-glia cell body condensation, determined by staining for neuron glia antigen-2/CSPG4 (NG2) and PDGFRα, commenced in the ischemic border of vehicle control brains at 3 hpi (Figure 3, D and E) and was significantly inhibited by imatinib treatment (Figure 3F). The majority of these $PDGFR\alpha^+$ NG2-glia cells expressed OLIG2, suggesting they are OPCs (Supplementary Figure S3, D and E). Since OPCs are progenitors of myelinating oligodendrocytes and our transcriptome analyses identified myelin basic protein, *Mbp*, as an imatinib-regulated gene (Supplementary Table 1 and 2, demonstrating downregulation at 3 hpi and upregulation at 24 hpi following imatinib treatment), we assessed expression of MBP in brain sections 3 hpi. These analyses did

however not detect any difference in myelination between imatinib-treated and control mice at 3 hpi (Supplementary Figure S3, F and G).

The reactive gliosis response also includes activation/recruitment of microglia/macrophages to the lesion site. Staining for CD11b, a marker for microglia/infiltrating macrophages, did however not show any difference in microgliosis/infiltrating macrophages at 3 hpi, and condensation of microglia was apparent in the ischemic border (arrows) of both vehicle- and imatinib-treated mice (Figure 3, G and H). The condensed $CD11b^+$ microglia co-expressed IBA1, another microglia/macrophage marker, but were negative for PDGFRα (Supplementary Figure S3H). Our analyses showed that the condensed $CD11b^+$;$IBA1^+$ microglia were often found in close proximity to $PDGFR\alpha^+$ cells (arrows, Supplementary Figure S3I), supporting efficient activation of PDGF-CC/PDGFRα signaling, which has been shown to be dependent on Mac-1 on microglia cells (36). Further analysis of the microglia/macrophage response to MCAO and imatinib treatment reveled that, in line with recent findings in rhesus monkeys (37), a high number of $CD68^+$ activated microglia/macrophages were detected in the ischemic border at 3 dpi, of which approximately 60% stained positive for the pro-fibrotic marker TGFβ in vehicle-treated animals (Figure 3, I-K). Imatinib treatment significantly reduced the number of TGFβ-expressing $CD68^+$ cells (Figure 3K), which is particularly interesting considering our data showing that PDGF-CC signaling regulates expression of genes in the TGFβ pathway (Figure 2, O and P). In addition, we found that imatinib significantly reduced the number of $CD11b^+$ ameboid microglia/infiltrating macrophages in the ischemic core at 7 dpi compared to controls (Supplementary Figure S3, J-L), whilst only displaying seemingly

limited effect on peripheral immune cell infiltration (neutrophil, B cell and T cell infiltration) (Supplementary Figure S4). Taken together this indicates that imatinib specifically attenuates the reactive gliosis response induced by MCAO with major effects seen on dampening activation of astrocytes, NG2-glia cells and microglia/macrophages.

Imatinib specifically targets myofibroblast expansion in the rim of the fibrotic scar

Since reactive gliosis has been suggested to orchestrate the subsequent formation of the glial and fibrotic scar (17) we next investigated whether the early effect of imatinib on reactive gliosis affected scar formation in the early chronic tissue remodeling phase at 7 dpi. Immunofluorescent stainings for the astroglia scar with GFAP (Figure 4A; Supplementary Figure S5A) and the NG2 glial scar (Figure 4B; Supplementary Figure S5B), respectively, revealed that imatinib treatment did not markedly affect glial scar formation. However, we found that, compared to vehicle controls, imatinib significantly reduced the formation and organization of a PDGFRα$^+$ scar (Figure 4, C-G), along the rim of a collagen 1 (COL1) rich fibrotic scar (Supplementary Figure S5, C-E). Our analyses revealed that the PDGFRα$^+$ scar was adjacent to the GFAP$^+$ scar, with some overlapping expression right at the border (arrows, Figure 4E). Further, we found that the PDGFRα$^+$ scar was embedded within the NG2$^+$ scar, although the majority of the parenchymal PDGFRα$^+$ cells in the fibrotic rim were negative for NG2 (two headed arrows, Figure 4, F and G) and OLIG2 (Supplementary Figure S5, F and G). We noted that the OLIG2$^+$ cells accumulated on the astroglia side of the scar and we detected no difference between imatinib and vehicle-treated mice. This was supported by stainings for MBP, revealing no

difference in MBP immunoreactivity between the two treatment groups (Supplementary Figure S5H).

To further characterize the fibrotic scar, we performed immunofluorescent stainings for the ECM glycoprotein fibronectin, a canonical myofibroblast gene (21). In line with the results from the gene expression analysis (Figure 2E), we found that imatinib reduced deposition of fibronectin (Figure 4H), this selectively in the highly-nucleated fibrotic rim without affecting the expression in the lesion core (Figure 4I; Supplementary Figure S5I). Co-staining for fibronectin and PDGFRα revealed that the PDGFRα$^+$ cells in the fibrotic rim were embedded within the fibronectin-positive ECM, suggesting that fibronectin is secreted by these cells (Figure 4J), thus indicating a myofibroblast identity of the PDGFRα$^+$ cells. Since parenchymal de novo expression of ASMA is a hallmark of myofibroblasts we investigated the expression of ASMA in the PDGFRα$^+$ fibrotic border at 7 dpi. We found that MCAO induced pronounced ectopic expression of ASMA in the PDGFRα$^+$ fibrotic rim of vehicle controls, which was significantly reduced by imatinib treatment (Figure 4, J-M; Supplementary Figure S5, J and K). Higher magnification images revealed that ASMA is co-expressed in these PDGFRα$^+$ cells indicating they are indeed myofibroblasts (two headed arrows) and we detected very few myofibroblasts in imatinib treated animals (Figure 4M). Contrary, ASMA expression in vascular smooth muscle cells (vSMC) appeared normal in both treatment groups and vSMCs did not co-express PDGFRα (arrows, Figure 4M; single confocal plane, Supplementary Figure S5K). It should be noted that in the unchallenged naïve brain, ASMA expression is restricted to vSMC surrounding medium-large sized vessels (arrow) and no parenchymal (non-vascular) expression is detected (asterisk, Supplementary Figure S5L). Staining with the

proliferation marker Ki67 showed high MCAO-induced proliferation within the fibrotic rim 7 dpi, which was non-significantly reduced following imatinib treatment (Supplementary Figure S5, M-O). Of note, our analyses showed that it was not only PDGFRα$^+$ myofibroblasts that proliferated in the fibrotic rim (as assessed from co-staining of Ki67 and PDGFRα. Arrowheads, Supplementary Figure S5N). Taken together this suggests that imatinib selectively inhibits myofibroblast expansion in the fibrotic rim after MCAO.

PDGFRα drives myofibroblast expansion in the fibrotic rim

Since imatinib is not only inhibiting signaling via PDGFRα but also PDGFRβ, we investigated the effect of imatinib on PDGFRβ which is abundantly expressed in the fibrotic scar after CNS injury (38, 39). Analysis of PDGFRβ expression in the lesion at 7 dpi showed that PDGFRβ immunoreactivity was detected throughout the lesion, with the highest signal detected in the fibrotic rim, adjacent to the GFAP astroglia border (Figure 5, A and B; Supplementary Figure S6A). Although, contrary to what we found with the PDGFRα$^+$ scar, the margin between the astroglia scar and the PDGFRβ$^+$ scar was not as distinct, with many activated astrocytes within the astroglia scar displaying de novo expression of PDGFRβ (asterisks, Figure 5B). Co-staining for PDGFRβ with PDGFRα and/or ASMA revealed that ASMA$^+$;PDGFRα$^+$ myofibroblasts co-expressed PDGFRβ (Figure 5, C and D; Supplementary Figure S6B). In fact, in vehicle controls we found that the vast majority of PDGFRβ$^+$ cells co-expressed PDGFRα and ASMA in the fibrotic rim, which would not only suggest that all myofibroblasts are PDGFRβ$^+$, but also that (nearly) all PDGFRβ$^+$ cells in the fibrotic rim are myofibroblasts. Surprisingly though, our analyses revealed that the thickness of the PDGFRβ$^+$ scar in the fibrotic rim was unaffected by imatinib treatment (Figure 5E), despite the fact that the PDGFRα$^+$;ASMA$^+$ scar was

consistently reduced (Figure 5, C and D). Further analyses of the myofibroblast scar demonstrated a population of PDGFRα^{+};PDGFRβ^{+} cells within the fibrotic rim adjacent to the GFAP^{+} astroglia scar with high expression of both receptors (referred to as PDGFRα^{high};PDGFRβ^{high}, two-headed arrows), while PDGFRα^{+};PDGFRβ^{+} cells located within the fibrotic rim but towards the fibrotic core exhibited lower expression of PDGFRα (referred to as PDGFRα^{low};PDGFRβ^{high}, arrowheads) (Figure 5C). Taken together our data suggest the existence of subpopulations of myofibroblasts within the fibrotic rim, possibly originating from different progenitor cells.

Based on the collective findings reported above, and the published data suggesting perivascular cells as the progenitors of myofibroblasts (40), we speculated that PDGFRα signaling in the NVU might be driving the expansion of the myofibroblast scar. To test this we utilized GFAP-Cre;PDGFRα flox mice, where PDGFRα is genetically ablated from GFAP expressing cells. This since in the non-ischemic murine brain, PDGFRα expression is, in addition to being expressed in NG2-glia cells (two-headed arrows), also detected in perivascular cells around medium-to-large sized vessels, where it is co-expressed with GFAP and PDGFRβ (arrows, Supplementary Figure S6, C-E). GFAP-Cre^{+};PDGFRα$^{flox/flox}$ mice have been shown to display a >60% reduction in perivascular PDGFRα signal in the murine brain compared to littermate controls (7). We found that loss of perivascular PDGFRα in GFAP-Cre^{+};PDGFRα$^{flox/flox}$ resulted in a significant reduction of the myofibroblast scar thickness in the fibrotic rim 7 dpi compared to littermate controls in which PDGFRα had not been ablated (GFAP-Cre^{-};PDGFRα$^{wt/wt}$, GFAP-Cre^{+};PDGFRα$^{wt/wt}$, GFAP-Cre^{-};PDGFRα$^{flox/flox}$) (Figure 5, F-H). Interestingly, the astroglia scar was unaffected in the GFAP-Cre^{+};PDGFRα$^{flox/flox}$ mice, suggesting different progenitors of the astroglia

and the myofibroblast scar, respectively. Thus, loss of PDGFRα signaling in perivascular cells is sufficient to diminish myofibroblast expansion.

Specific inhibition of PDGF-CC/PDGFRα signaling reduces stroke lesion volume and myofibroblast expansion in the fibrotic scar

To further investigate the role of PDGFRα in myofibroblast expansion after MCAO we made use of a monoclonal anti-human PDGF-CC antibody that neutralizes PDGF-CC, the ligand for PDGFRα, in genetically modified mice expressing a humanized form of PDGF-CC (PDGF-CC^{hum}) (25, 26). This allowed us to exclusively inhibit PDGF-CC/PDGFRα signaling, without affecting PDGFRβ signaling or any of the other targets of imatinib. We found that at 3 dpi, infarct volume was significantly reduced in the animals receiving anti-PDGF-CC antibody treatment compared to animals treated with the control antibody (Figure 6A). This coincided with reduced weight loss, indicative of a better general condition, in anti-PDGF-CC antibody treated animals (Figure 6B). Assessment of myofibroblast scar thickness at 7 dpi showed a significant reduction in animals treated with the anti-PDGF-CC antibody compared to controls (Figure 6, C-F). Like with imatinib, the astroglia scar (Supplementary Figure S7, A and B), and the NG2 glial scar (Supplementary Figure S7, C and D) appeared unaffected by anti-PDGF-CC antibody treatment. Staining for Ki67 we found extensive proliferation in the fibrotic rim 7 dpi of control antibody treated mice, which was significantly reduced in anti-PDGF-CC antibody treated animals (Figure 6, G-I; Supplementary Figure S7E). To determine whether the effect of anti-PDGF-CC antibody treatment on the myofibroblast scar was mediated via PDGFRα, we assessed PDGFRα activation at 6 hpi and 7 dpi by

immunofluorescent stainings using two different antibodies that recognize specific phosphorylation sites on activated PDGFRα (pY754 and pY1018) (36, 41). Both antibodies detected phosphorylation of PDGFRα around vessels at 6 hpi in control animals, which was significantly reduced in animals treated with the anti-PDGF-CC antibody compared to controls (pY1018, Figure 6, J and K and Supplementary Figure S7F; pY754, Supplementary Figure S7, G-I). At 7 dpi, a strong PDGFRα phosphorylation signal was detected in the PDGFRα$^+$ fibrotic rim of control treated animals, whereas this was markedly reduced in anti-PDGF-CC antibody treated animals (pY1018, Figure 6, L and M and Supplementary Figure S7, J and K; pY754, Supplementary Figure S7, L and M). In summary these data show that selective inhibition of the PDGF-CC/PDGFRα signaling pathway results in the reduction of stroke infarct volume and myofibroblast expansion similar to that seen with imatinib treatment, thus potentially offering a targeted treatment approach for patients suffering from ischemic stroke.

Imatinib progressively improves function in a sensory-motor integration test after MCAO

To test how reduced BBB breach and myofibroblast expansion, after *pre-* or *post-treatment* with imatinib, affects functional recovery we assessed a lateralized sensory-motor integration test at 3 dpi and 7 dpi using the corridor task modified for mice (30, 42, 43) (see experimental outline in Figure 7A). This test is based on the fact that unilateral brain lesions will cause contralateral neglect and thus, lead to a preference to explore/retrieve objects or food placed on the side ipsilateral to the lesion (ipsilateral bias). Functional improvement after a treatment will therefore result in reduced

ipsilateral bias. Analysis of the PDGFRα⁺ scar in *post-infarct-treated* mice, which received their first dose of imatinib 24 hours after MCAO and thus had experienced the first wave of MCAO-induced BBB leakage, revealed that *post-treatment* still resulted in a significant reduction in PDGFRα⁺ scar thickness (Figure 7B; Supplementary Figure S8A). The reduction in PDGFRα⁺ scar thickness was equal to the effect seen after imatinib *pre-treatment* (Figure 4D), indicating that scar expansion was largely independent of the early BBB disruption. Using the corridor test, we found that at 3 dpi and 7 dpi all vehicle-treated mice preferentially explored sugar pellets on the side ipsilateral to the lesion (Figure 7C and Video S1) and did not display any functional recovery over time (Figure 7D). Imatinib *post-treatment* significantly reduced ipsilateral exploration bias compared to vehicle controls at 7 dpi, but not at 3 dpi (Figure 7C). Imatinib *pre-treated* animals on the other hand, displayed significantly reduced ipsilateral bias already at 3 dpi, which was further improved at 7 dpi (Figure 7C). Further analysis showed that both imatinib *pre-* and *post-treated* animals displayed about 50% functional improvement between 3 dpi and 7 dpi (Figure 7D). Analysis of infarct volume at 7 dpi revealed that imatinib *pre-* and *post-treated* animals displayed similar lesion sizes (Figure 7E) and that infarct size significantly correlated with exploration bias (Figure 7F). This correlation between infarct size and exploration bias is further supported by the fact that no difference was detected in either infarct volume (Supplementary Figure S8B) or exploration bias (Figure 7C) comparing imatinib *post-treated* animals to vehicle controls at 3 dpi. Using two-photon microscopy, we followed vascular perfusion over time in the ischemic area of untreated and imatinib *pre-treated* animals from before onset of ischemia to 7 dpi (Figure 7, G and H). Our analyses showed that, while there was no improvement in vessel perfusion between 3 dpi and 7 dpi in control animals, vessel perfusion increased significantly in the

imatinib-treated cohort in the same time frame (Figure 7H). This correlated well with exploration bias (Figure 7C), thus suggesting that vessel perfusion might contribute to the improvement in functional outcome seen in imatinib-treated animals. However, it should be noted that at 3 dpi we detected no difference in vascular perfusion comparing untreated and imatinib *pre-treated* animals (Figure 7H), even though functional improvement was detected following *pre-treatment* with imatinib at this timepoint (Figure 7C). Taken together this suggests that late and continued intervention to block the PDGF-CC/PDGFRα signaling pathway might improve functional recovery by limiting myofibroblast scar formation.

Discussion

We have previously shown that PDGF-CC/PDGFRα signaling regulates cerebrovascular permeability in a tPA-dependent manner, and that inhibiting disease-induced BBB breakdown by targeting this pathway with imatinib significantly improves outcome in a number of experimental disease models (5-11). Yet, how targeting the BBB translates into improved neurological outcome is poorly understood and the current literature indicates a complex relationship between disease-induced BBB breakdown and CNS repair (4, 17, 44). Here we present data that imatinib pre-treatment (administered before induction of ischemia and disease-induced BBB breach) accelerated the functional recovery after MCAO compared to imatinib post-treatment (administered 24 hours after induction of ischemia and the first peak of disease-induced BBB breach had subsided). Importantly though, despite the fact that post-treatment is not targeting the first wave of BBB breach nor the acute reactive gliosis response, imatinib post-treated mice reached the same level of functional recovery as imatinib pre-treated mice at 7 dpi. Our data thus indicate a much sought after therapeutic strategy that can help restore brain function in the post-acute phase of ischemic stroke when current treatment options are limited to rehabilitation therapies.

In addition to regulating BBB integrity, we found that imatinib dampened MCAO-induced expression of pro-fibrotic/pro-inflammatory genes in the cerebrovasculature and diminished myofibroblast expansion in the rim of the fibrotic scar after MCAO. This is of particular interest considering that the fibrotic component of the CNS scar has recently emerged as a potential target in CNS repair, and that a moderate and region-specific

reduction of fibrotic scarring, which still allows wound closure, promotes axon regeneration and functional recovery in experimental models of spinal cord injury (SCI) (45) and multiple sclerosis (EAE) (46). Based on this we hypothesize that modulation of the myofibroblast response, by targeting signaling via PDGFRα, contributes to the beneficial effect seen on neurological and functional outcome with imatinib after ischemic stroke (9, 15). This is supported by a line of evidence, including studies showing that PDGF-CC/PDGFRα signaling is associated with fibrotic- and myofibroblast expansion in other organs (23, 47-51) and that ablation of PDGFRα in myofibroblast progenitor cells reduces myofibroblast differentiation and improves liver function in a model of liver disease (49), while sustained myofibroblast expansion is detrimental to healing processes (21). Importantly, we found that TGFβ, which is a key factor stimulating myofibroblast differentiation (21), was upregulated in the cerebrovasculature following PDGF-CC administration and downregulated following imatinib treatment in disease-associated microglia/macrophages. Lastly, our data show that imatinib reduced MCAO-induced expression of the canonical myofibroblast gene fibronectin. Fibronectin is known to decrease neuronal growth cone velocity in vitro (52) and contribute to remyelination failure within multiple sclerosis lesions (53), thus suggesting that a fibronectin dense scar might interfere with axon regeneration whilst decreased fibronectin deposition could ameliorate functional recovery. Further experiments will however be needed to fully understand the functional contribution of the myofibroblast scar to CNS recovery and to delineate the exact mechanism by which PDGF-CC/PDGFRα signaling is involved in this process.

The proposed progenitors of myofibroblasts include circulating bone marrow-derived fibrocytes (54, 55); tissue-resident/meningeal/choroid-plexus fibroblasts (56) and other mesenchymal cells related to blood vessels, e.g. pericytes, which could differentiate via epithelial-/endothelial-to-mesenchymal transition (40). In the CNS, lineage tracing analyses largely supports the latter, i.e. that perivascular cells in the NVU are the main progenitors of the fibrotic (39, 57) and myofibroblast scar formation (58), of which a subset resides along medium-to-large sized vessels and expresses PDGFRα and PDGFRβ. These studies suggest that activated perivascular cells leave the vessel wall in the acute phase following ischemia, after which they migrate/ proliferate/ differentiate to form the myofibroblast scar in the chronic phase after ischemia. Thus, blocking the initial activation of the perivascular cells would stop them from leaving the vessel wall, subsequently leading to fewer cells that could proliferate/ differentiate and populate the myofibroblast scar. Our data suggest the existence of subpopulations of myofibroblasts within the fibrotic rim, of which some myofibroblasts expressed high levels of PDGFRα (PDGFRα^{high};PDGFRβ^{high}) while others displayed low expression (PDGFRα^{low};PDGFRβ^{high}). Myofibroblasts with high expression levels of PDGFRα localized adjacent to the astroglial scar, while those with low expression levels of PDGFRα were found closer to the fibrotic core. It is possible that these subpopulations arise from multiple progenitors and that they exert different effects in the healing response after ischemic stroke. This is supported by recent findings showing that myofibroblasts arise from multiple progenitors after SCI (58) and that different subpopulations of myofibroblasts elicit different protective/harmful functions in repair processes (59). It is however also possible that the PDGFRα^{low};PDGFRβ^{high} and PDGFRα^{high};PDGFRβ^{high} cells represent different stages of myofibroblast maturation. Thus, imatinib might block the

differentiation into fully maturated myofibroblasts, whilst the number of progenitor cells remains the same. Understanding the temporo-spatial regulation as well as the cellular origin/potential multilineage differentiation of the injury-induced myofibroblasts are central to allow for future manipulation of the fibrotic scar.

The cellular identity of the perivascular PDGFRα$^+$ cells is not completely elucidated, and these cells have been referred to in the literature as fibroblast-like cells (56, 60), type A pericytes (57), perivascular stromal cells (61) and by us as perivascular astrocytes (based on co-expression with GFAP and AQP4) (7-10, 30, 36). Whether these names are referring to the same population or different subpopulations of cells remains to be determined. Nevertheless our studies, utilizing GFAP-Cre:PDGFRα flox mice, which display a > 60% reduction in perivascular PDGFRα signal in the murine brain (7), or a monoclonal anti-PDGF-CC antibody (25), clearly demonstrate that genetic ablation of PDGFRα in GFAP positive cells or pharmacologic neutralization of the ligand for PDGFRα result in a diminished myofibroblast scar. This suggests that PDGFRα signaling is critical for the expansion of the myofibroblast scar. Contrary, our analyses suggests that PDGFRβ, which is also inhibited by imatinib, constitutes a marker of myofibroblasts/their progenitors and does not drive the expansion of the myofibroblast scar. However, since PDGFRβ is co-expressed in the potential perivascular PDGFRα$^+$ progenitor cells and myofibroblasts, and PDGF-CC can induce signaling via the heterodimeric receptor PDGFRαβ, it is tempting to speculate that signaling via PDGFRαα homodimers and PDGFRαβ heterodimers might be of importance for myofibroblast expansion, but that they might trigger distinguished cellular responses.

In line with previous work (37), we detected a great number of TGFβ-expressing $CD68^+$ cells in the ischemic area, presumably microglia/macrophages although it should be noted that bone-marrow derived fibrocytes also express CD68 (54) and are capable of acquiring myofibroblast characteristics (55). Our data demonstrate that imatinib reduced expression of TGFβ in these $CD68^+$ cells and attenuated MCAO-induced cerebrovascular expression of *Itgax* (encoding CD11c). Since TGFβ is a key regulator of myofibroblast differentiation (21) and *Itgax* is a well-known disease associated microglia gene (62), our data infer a direct immune system-fibrosis crosstalk in ischemic stroke. In support of this are studies demonstrating that macrophages promote myofibroblast expansion in skin repair (63) and that fibroblasts coordinate neuroinflammation after brain injury (64). Further, TGFβ-PDGFRα crosstalk (22) and macrophage-expressed PDGF-CC (65) have been implicated in myofibroblast scar expansion in other organs, and we found that efficient proteolytic activation of PDGF-CC requires the integrin Mac1 on microglia (36). The fibrotic scar has been shown to play a role in regulating disease severity during neuroinflammation in EAE (46) and interestingly, we have previously shown that imatinib and anti-PDGF-CC antibody treatment can ameliorate EAE severity (6, 11). Originally we ascribed the beneficial effect of anti-PDGF-CC/PDGFRα treatment in EAE to the attenuation of disease-provoked BBB breakdown, but it is possible that inhibiting the PDGF-CC/PDGFRα pathway also targets the fibrotic response in EAE.

Taken together, we here provide evidence of what we believe to be a novel way to modify the myofibroblast scar by targeting PDGFRα signaling, either with imatinib or with a monoclonal anti-PDGF-CC antibody. Importantly, our findings demonstrate improved functional recovery following subacute administration of imatinib which might be of

great importance given the current lack of post-acute treatment options for ischemic stroke patients.

Materials and methods

Sex as a biological variable.

Sex as a biological variable was considered by making use of both male and female animals. Similar findings were seen in both sexes.

Animals

Wild-type C57BL/6 (Charles River), C57BL/6NTac-Pdgfc$^{tm3633(K242T,\ K246R,\ R299S,\ K318R,\ N342S,\ A343T)Arte}$ (referred to as PDGF-CC^{hum} mice) (26), GFAP-Cre;PDGFRα^{flox} (7) and Cldn5(BAC)-GFP mice (24, 60, 66), aged 2-7 months, were used in this study. PDGF-CC^{hum} mice express a humanized growth factor domain which allows neutralizing PDGF-CC signaling using a murine anti-human PDGF-CC antibody (25, 26). GFAP-Cre;PDGFRα^{flox} mice express Cre-recombinase under the murine GFAP promoter (67) and loxP sites flanking exon 2 and 3 of the PDGFRα gene (68). Cldn5(BAC)-GFP mice express cytosolic GFP under the claudin5 promoter leading to endogenous labeling of endothelial cells.

Experimental ischemic stroke model

A photothrombotic model of middle cerebral artery occlusion (MCAO), using the photoactivatable dye Rose Bengal and light activation with a laser at the level of the surgically exposed middle cerebral artery (MCA), was used as a model for experimental ischemic stroke. Details are presented in the Supplemental Materials and Methods.

Imatinib treatment

Mice were treated with imatinib (Novartis, alternatively Mylan AB) by oral gavage (details on the preparation are presented in the Supplemental Materials and Methods). Mice *pre-treated* with imatinib received three doses (morning-night-morning) before MCAO, and were then treated twice daily until the end of the experiment. In *post-treated* animals imatinib treatment was initiated 24 hpi and then treated twice daily until the end of the experiment. As controls, mice were gavaged the corresponding times with vehicle (H_2O for the functional corridor tests, PBS for all other experiments), except for the two-photon imaging experiments in which the control animals were untreated.

Anti-PDGF-CC antibody treatment

Homozygous PDGF-CC^{hum} mice were intraperitoneally injected with a single dose of 2 mg/ml of either murine anti-human PDGF-CC (mu6B3, a kind gift from Paracrine Therapeutics AB as described in (25)) or control antibody (IgG2a clone C1.18.4, BioXcell) in PBS (resulting in 400 μg per mouse) the day before MCAO induction. For experiments longer than 3 days, a second dose was given 3 dpi.

Two-photon imaging

Cranial window implantation over the cortical branch of the middle cerebral artery, stroke induction through the cranial window, two-photon imaging and image analysis were performed as previously described (24) (details are presented in the Supplemental Materials and Methods).

Evans blue (EB) dye extravasation

BBB breakdown in the ipsilateral hemisphere at different time points after MCAO was assessed by extravasation of Evans blue dye as previously described (9, 36, 69) (details are presented in the Supplemental Materials and Methods).

Immunohistochemistry

Tissue preparation of fixed or fresh-frozen brains for sectioning, immunofluorescent stainings and confocal image acquisition were conducted using standard protocols. Details, lists of antibodies and image analyses can be found in Supplemental Materials and Methods.

Intracerebroventricular injection (ICV)

Vehicle or active PDGF-CC were injected into the left lateral ventricle of naïve C57BL/6 mice. 4 h after ICV, brains were rapidly dissected out and used for isolation of cerebrovascular fragments. Details are presented in the Supplemental Materials and Methods.

Isolation of cerebrovascular fragments, generation of mRNA and real-time quantitative PCR analysis

Cerebrovascular fragments were isolated with antibody-coupled magnetic beads as previously described (30, 70). RNA was extracted and used for mRNA expression array analysis and cDNA generation for real-time quantitative PCR analysis. Methodological details and a list of primers are presented in the Supplemental Materials and Methods.

Microarray and data analysis

GeneChip® ST Arrays (GeneChip® Mouse Gene 2.0 ST Array) were hybridized with cDNA from cerebrovascular fragments and washed, stained and scanned. Differential gene expression for molecules from the dataset that met the < or > log2 (0.5) fold change and *P*-value < 0.05 cutoff in cerebrovascular fragments from imatinib- and vehicle-treated mice were compared using the ingenuity pathways analysis platform (Qiagen). The molecules in this dataset were grouped in biological functions and/or diseases or were associated with a canonical pathway in Ingenuity's knowledge base. To compare our dataset to the harmonizome database (31), we used the dataset "fibrosis, CTD Gene-Disease Associations" and compared our dataset with all genes from the fibrosis dataset showing a higher standardized value than 1,5. Details are presented in the Supplemental Materials and Methods.

Corridor task and stroke volume

Assessment of functional recovery by measuring lateralized sensory-motor integration using a corridor task was done as previously described (30). Infarct volume analysis with 4% 2,3,5-triphenyltetrazolium chloride (TTC) staining was performed as described previously (9, 36).

Statistics

Data analysis was performed using GraphPad Prism 9 statistical software. For statistical analysis in experiments with only two groups a two-tailed, paired or unpaired t-test with Welch's correction was used. For experiments with more than two groups, statistical

evaluation correcting for multiple comparisons and/or repeated measures was performed as stated in the figure legend with statistical significance defined as $*P \leq 0.05$, $**P \leq 0.01$ and $***P \leq 0.001$. Data is presented as mean values ± SEM.

Study approval

All experiments in this study were approved and performed in accordance with the guidelines from the Swedish National Board for Laboratory Animals and the European Community Council Directive (86/609/EEC) and were approved by the North Stockholm Animal Ethics Committee and the Institutional Animal Care and Use Committee of Unit for Laboratory Animal Medicine at the University of Michigan, respectively.

Data availability

Data are available in the Supporting Data Values file. Raw data of the microarrays are deposited on the NCBI Gene Expression Omnibus database (accession no. GSE137534).

Author contributions

LF and JP designed the study and wrote the manuscript with critical input from MZ and DAL and all the co-authors; UE contributed critical resources; JP, MZ, CS, DT, MZA, KM, SR, SAL, LM, IN, EJS and LF conducted experiments and acquired data; JP, MZ, CS, DT, MZA, IN and LF analyzed data.

Acknowledgements

This work was supported by the Karolinska Institutet (MZ, MZA, UE, IN, LF), the Swedish Research Council (Vetenskapsrådet) (LF, 524-2010-7045; 521-2012-1853)(UE, 2016-02593; 2017-01794; 2017-00691)(IN, FS-2008-90)(SAL, 2021-02605), the Swedish Governmental Agency for Innovation Systems (VINNOVA) (LF, 2011-03503), Hållsten research foundation (UE, IN, LF), Swedish Brain Foundation (UE, IN, LF, FO2020-0037; FO2021-0039)(SAL., FO2022-0233),), FSG FANG FOUNDATION (UE, IN, LF), Ulla Hamberg Angeby och Lennart Angebys stiftelse (LF), Torsten Söderberg Foundation (UE, M137/16), Neurofonden (MZ, MZA, SAL, IN) , Biogen Idec, Inc. (MZA), Region Stockholm (MZA, ALF project, 20180181), Tore Nilsons Stiftelse (MZA), Åhlen foundation (SAL), the Royal Swedish Academy of Sciences (IN), Magnus Bergvall´s foundation (IN), the Swedish Stroke Association/STROKE Riksförbundet (IN), and the Swedish Heart and Lung foundation (Hjärt-lungfonden)(UE, IN, 20150547), the National Institutes of Health, HL055374, and AG074552 (DAL). We would like to thank the Array and Analysis Facility, Science for Life Laboratory at Uppsala Biomedical Center (BMC), Husargatan 3, 751 23 Uppsala; Yihang Li and Nadine Winkler for help with qPCR and stainings, and Christer

Betsholtz (Uppsala University, Uppsala, Sweden) for kindly providing Cldn5(BAC)-GFP mice.

Supplementary material

Supplementary material is available at Journal of Clinical Investigation online.

References

1. Saini V, et al. Global Epidemiology of Stroke and Access to Acute Ischemic Stroke Interventions. *Neurology.* 2021;97(20 Suppl 2):S6-S16.

2. Prabhakaran S, et al. Acute stroke intervention: a systematic review. *JAMA.* 2015;313(14):1451-62.

3. Abdullahi W, et al. Blood-brain barrier dysfunction in ischemic stroke: targeting tight junctions and transporters for vascular protection. *Am J Physiol Cell Physiol.* 2018;315(3):C343-C56.

4. Stanimirovic DB, Friedman A. Pathophysiology of the neurovascular unit: disease cause or consequence? *J Cereb Blood Flow Metab.* 2012;32(7):1207-21.

5. Abrams MB, et al. Imatinib enhances functional outcome after spinal cord injury. *PLoS One.* 2012;7(6):e38760.

6. Adzemovic MZ, et al. Imatinib ameliorates neuroinflammation in a rat model of multiple sclerosis by enhancing blood-brain barrier integrity and by modulating the peripheral immune response. *PLoS One.* 2013;8(2):e56586.

7. Fredriksson L, et al. Identification of a neurovascular signaling pathway regulating seizures in mice. *Ann Clin Transl Neurol.* 2015;2(7):722-38.

8. Lewandowski SA, et al. Presymptomatic activation of the PDGF-CC pathway accelerates onset of ALS neurodegeneration. *Acta Neuropathol.* 2016;131(3):453-64.

9. Su EJ, et al. Activation of PDGF-CC by tissue plasminogen activator impairs blood-brain barrier integrity during ischemic stroke. *Nat Med.* 2008;14(7):731-7.

10. Su EJ, et al. Imatinib treatment reduces brain injury in a murine model of traumatic brain injury. *Front Cell Neurosci.* 2015;9.

11. Zeitelhofer M, et al. Blocking PDGF-CC signaling ameliorates multiple sclerosis-like neuroinflammation by inhibiting disruption of the blood-brain barrier. *Sci Rep*. 2020;10(1):22383.

12. Iqbal N, Iqbal N. Imatinib: a breakthrough of targeted therapy in cancer. *Chemother Res Pract*. 2014;2014:357027.

13. Ma Q, et al. PDGFR-alpha inhibition preserves blood-brain barrier after intracerebral hemorrhage. *Ann Neurol*. 2011;70(6):920-31.

14. Merali Z, et al. Longitudinal assessment of imatinib's effect on the blood-brain barrier after ischemia/reperfusion injury with permeability MRI. *Transl Stroke Res*. 2015;6(1):39-49.

15. Wahlgren N, et al. Randomized assessment of imatinib in patients with acute ischaemic stroke treated with intravenous thrombolysis. *J Intern Med*. 2017;281(3):273-83.

16. Robel S, et al. The stem cell potential of glia: lessons from reactive gliosis. *Nat Rev Neurosci*. 2011;12(2):88-104.

17. Burda JE, Sofroniew MV. Reactive gliosis and the multicellular response to CNS damage and disease. *Neuron*. 2014;81(2):229-48.

18. Pekny M, et al. The dual role of astrocyte activation and reactive gliosis. *Neurosci Lett*. 2014;565:30-8.

19. Anderson MA, et al. Astrocyte scar formation aids central nervous system axon regeneration. *Nature*. 2016;532(7598):195-200.

20. Shechter R, Schwartz M. CNS sterile injury: just another wound healing? *Trends Mol Med*. 2013;19(3):135-43.

21. Hinz B. Formation and function of the myofibroblast during tissue repair. *J Invest Dermatol*. 2007;127(3):526-37.

22. Contreras O, et al. Cross-talk between TGF-beta and PDGFRalpha signaling pathways regulates the fate of stromal fibro-adipogenic progenitors. *J Cell Sci*. 2019;132(19).

23. Yao L, et al. Temporal control of PDGFRalpha regulates the fibroblast-to-myofibroblast transition in wound healing. *Cell Rep*. 2022;40(7):111192.

24. Protzmann J, et al. Analysis of ischemic stroke-mediated effects on blood-brain barrier properties along the arteriovenous axis assessed by intravital two-photon imaging. *Fluids Barriers CNS*. 2024;21(1):35.

25. Li H, et al. Development of monoclonal anti-PDGF-CC antibodies as tools for investigating human tissue expression and for blocking PDGF-CC induced PDGFRalpha signalling in vivo. *PLoS One*. 2018;13(7):e0201089.

26. Zeitelhofer M, et al. Preclinical toxicological assessment of a novel monoclonal antibody targeting human platelet-derived growth factor CC (PDGF-CC) in PDGF-CChum mice. *PLoS One*. 2018;13(7):e0200649.

27. Yang Y, Rosenberg GA. Blood-brain barrier breakdown in acute and chronic cerebrovascular disease. *Stroke*. 2011;42(11):3323-8.

28. Knowland D, et al. Stepwise recruitment of transcellular and paracellular pathways underlies blood-brain barrier breakdown in stroke. *Neuron*. 2014;82(3):603-17.

29. Krueger M, et al. Blood-brain barrier breakdown after embolic stroke in rats occurs without ultrastructural evidence for disrupting tight junctions. *PLoS One*. 2013;8(2):e56419.

30. Goncalves A, et al. Thrombolytic tPA-induced hemorrhagic transformation of ischemic stroke is mediated by PKCbeta phosphorylation of occludin. *Blood*. 2022;140(4):388-400.

31. Rouillard AD, et al. The harmonizome: a collection of processed datasets gathered to serve and mine knowledge about genes and proteins. *Database (Oxford)*. 2016 Jul 3;2016:baw100.

32. Domingues S. Expression data from human brain samples, geo, V1. https://www.ncbi.nlm.nih.gov/geo/query/acc.cgi?acc=GSE24265. 2010. Updated Mar 25, 2019. Accessed Mar 2022.

33. Chen Y, et al. Perihematomal Edema After Intracerebral Hemorrhage: An Update on Pathogenesis, Risk Factors, and Therapeutic Advances. *Front Immunol.* 2021;12:740632.

34. Xu J, et al. TGF-beta-induced epithelial to mesenchymal transition. *Cell Res.* 2009;19(2):156-72.

35. Sofroniew MV. Astrocyte barriers to neurotoxic inflammation. *Nat Rev Neurosci.* 2015;16(5):249-63.

36. Su EJ, et al. Microglial-mediated PDGF-CC activation increases cerebrovascular permeability during ischemic stroke. *Acta Neuropathol.* 2017;134(4):585-604.

37. Yeo HG, et al. Increased CD68/TGFbeta Co-expressing Microglia/ Macrophages after Transient Middle Cerebral Artery Occlusion in Rhesus Monkeys. *Exp Neurobiol.* 2019;28(4):458-73.

38. Dias DO, Goritz C. Fibrotic scarring following lesions to the central nervous system. *Matrix Biol.* 2018;68-69:561-70.

39. Dias DO, et al. Pericyte-derived fibrotic scarring is conserved across diverse central nervous system lesions. *Nat Commun.* 2021;12(1):5501.

40. Di Carlo SE, Peduto L. The perivascular origin of pathological fibroblasts. *J Clin Invest.* 2018;128(1):54-63.

41. Rupp E, et al. A unique autophosphorylation site in the platelet-derived growth factor alpha receptor from a heterodimeric receptor complex. *Eur J Biochem.* 1994;225(1):29-41.

42. Dowd E, et al. The Corridor Task: a simple test of lateralised response selection sensitive to unilateral dopamine deafferentation and graft-derived dopamine replacement in the striatum. *Brain Res Bull.* 2005;68(1-2):24-30.

43. Grealish S, et al. Characterisation of behavioural and neurodegenerative changes induced by intranigral 6-hydroxydopamine lesions in a mouse model of Parkinson's disease. *Eur J Neurosci.* 2010;31(12):2266-78.

44. Profaci CP, et al. The blood-brain barrier in health and disease: Important unanswered questions. *J Exp Med.* 2020;217(4).

45. Dias DO, et al. Reducing Pericyte-Derived Scarring Promotes Recovery after Spinal Cord Injury. *Cell.* 2018;173(1):153-65 e22.

46. Dorrier CE, et al. CNS fibroblasts form a fibrotic scar in response to immune cell infiltration. *Nat Neurosci.* 2021;24(2):234-44.

47. Eitner F, et al. PDGF-C is a proinflammatory cytokine that mediates renal interstitial fibrosis. *J Am Soc Nephrol.* 2008;19(2):281-9.

48. Grun K, et al. Elevated expression of PDGF-C in coxsackievirus B3-induced chronic myocarditis. *Eur Heart J.* 2005;26(7):728-39.

49. Kikuchi A, et al. Hepatic Stellate Cell-Specific Platelet-Derived Growth Factor Receptor-alpha Loss Reduces Fibrosis and Promotes Repair after Hepatocellular Injury. *Am J Pathol.* 2020;190(10):2080-94.

50. Zhuo Y, et al. Modulation of PDGF-C and PDGF-D expression during bleomycin-induced lung fibrosis. *Am J Physiol Lung Cell Mol Physiol.* 2004;286(1):L182-8.

51. Varone F, et al. Nintedanib for the treatment of idiopathic pulmonary fibrosis. *Expert Opin Pharmacother.* 2018;19(2):167-75.

52. Kuhn TB, et al. Laminin and fibronectin guideposts signal sustained but opposite effects to passing growth cones. *Neuron.* 1995;14(2):275-85.

53. Stoffels JM, et al. Fibronectin aggregation in multiple sclerosis lesions impairs remyelination. *Brain.* 2013;136(Pt 1):116-31.

54. Mitsuhashi A, et al. Identification of fibrocyte cluster in tumors reveals the role in antitumor immunity by PD-L1 blockade. *Cell Rep.* 2023;42(3):112162.

55. Aldrich A, Kielian T. Central nervous system fibrosis is associated with fibrocyte-like infiltrates. *Am J Pathol.* 2011;179(6):2952-62.

56. Pietila R, et al. Molecular anatomy of adult mouse leptomeninges. *Neuron*. 2023;111(23):3745-64 e7.

57. Goritz C, et al. A pericyte origin of spinal cord scar tissue. *Science*. 2011;333(6039):238-42.

58. Holl D, et al. Distinct origin and region-dependent contribution of stromal fibroblasts to fibrosis following traumatic injury in mice. *Nat Neurosci*. 2024;27(7):1285-98.

59. Sinha S, et al. Fibroblast inflammatory priming determines regenerative versus fibrotic skin repair in reindeer. *Cell*. 2022;185(25):4717-36 e25.

60. Vanlandewijck M, et al. A molecular atlas of cell types and zonation in the brain vasculature. *Nature*. 2018;554(7693):475-80.

61. Kelly KK, et al. Col1a1+ perivascular cells in the brain are a source of retinoic acid following stroke. *BMC Neurosci*. 2016;17(1):49.

62. Deczkowska A, et al. Disease-Associated Microglia: A Universal Immune Sensor of Neurodegeneration. *Cell*. 2018;173(5):1073-81.

63. Shook BA, et al. Myofibroblast proliferation and heterogeneity are supported by macrophages during skin repair. *Science*. 2018;362(6417).

64. Ewing-Crystal NA, et al. Dynamic fibroblast-immune interactions shape wound healing after brain injury [preprint]. https://doi.org/10.1101/2024.03.13.584873. Posted on bioRxiv March 15, 2024.

65. Glim JE, et al. Platelet derived growth factor-CC secreted by M2 macrophages induces alpha-smooth muscle actin expression by dermal and gingival fibroblasts. *Immunobiology*. 2013;218(6):924-9.

66. Wang Y, et al. Characterization of multi-cellular dynamics of angiogenesis and vascular remodelling by intravital imaging of the wounded mouse cornea. *Sci Rep*. 2018;8(1):10672.

67. Garcia AD, et al. GFAP-expressing progenitors are the principal source of constitutive neurogenesis in adult mouse forebrain. *Nat Neurosci*. 2004;7(11):1233-41.

68. Tallquist MD, Soriano P. Cell autonomous requirement for PDGFRalpha in populations of cranial and cardiac neural crest cells. *Development.* 2003;130(3):507-18.

69. Yepes M, et al. Tissue-type plasminogen activator induces opening of the blood-brain barrier via the LDL receptor-related protein. *J Clin Invest.* 2003;112(10):1533-40.

70. Bondjers C, et al. Microarray analysis of blood microvessels from PDGF-B and PDGF-Rbeta mutant mice identifies novel markers for brain pericytes. *FASEB J.* 2006;20(10):1703-5.

Figures and Figure legends

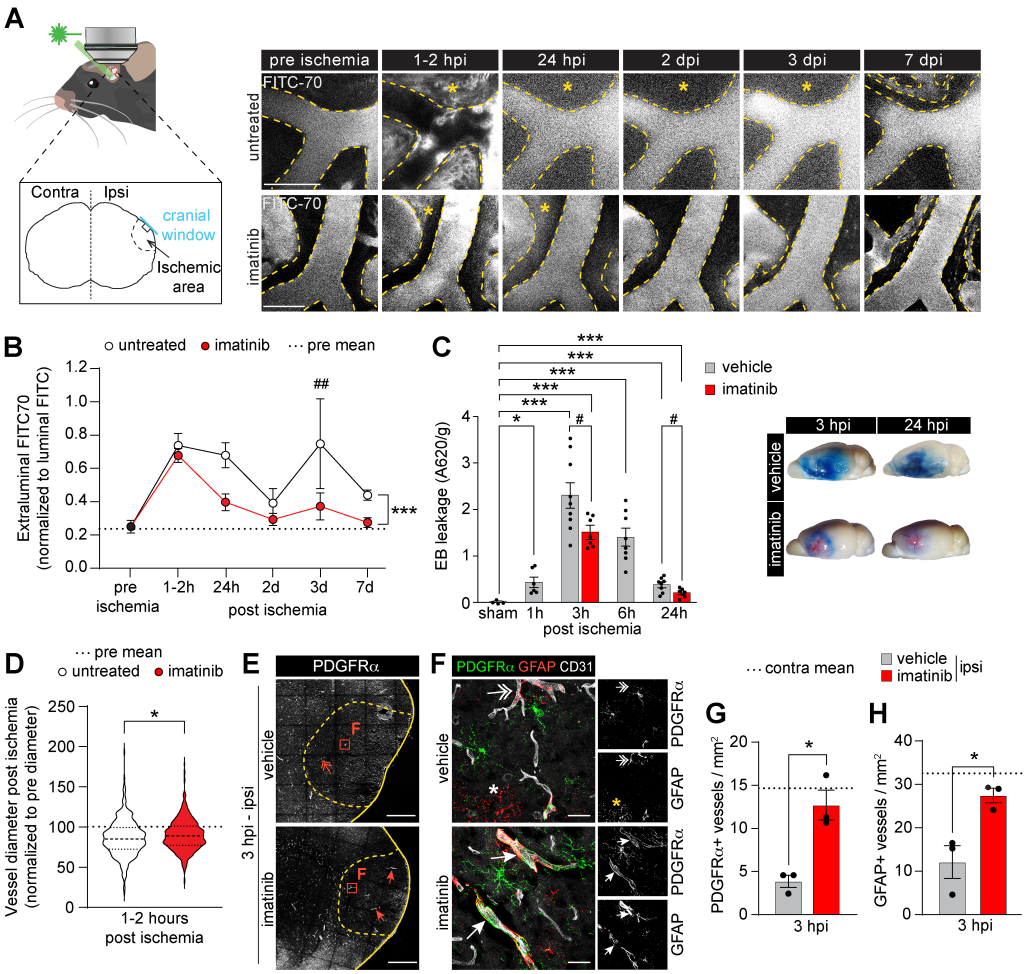

Figure 1. Imatinib attenuates MCAO-induced cerebrovascular breach and vasoconstriction. (**A**) Two-photon images of FITC70 signal before ischemia (pre) and at different time points after ischemia. Asterisks, extraluminal FITC70 signal. (**B**) Quantification of two-photon extraluminal FITC70 signal (*N* = 4). *Treatment effect; #relative to control at that time point. (**C**) Analysis and representative images of Evans blue (EB) extravasation in the ipsilateral ischemic hemisphere in the acute phase after MCAO (*N* = 4-9). *Relative to sham; #Relative to vehicle controls. (**D**) Quantification of relative vessel diameter change 1-2 hpi compared to the diameter before onset. Recorded with longitudinal two-photon microscopy in endothelial reporter mice (*N* = 399 (untreated); 609 (imatinib) vessels from 4 animals per treatment. (**E** and **F**) Ipsilateral overviews (**E**) and high-magnifications from the ischemic area (**F**) of immunofluorescent stainings for PDGFRα and GFAP in brain sections collected at 3 hpi. Vessels were visualized with CD31. Arrows, perivascular expression of PDGFRα and GFAP; Two-headed arrows, scattered/lost perivascular expression of PDGFRα and GFAP; Asterisk, non-perivascular GFAP signal. Ischemic area outlined with dashed lines. (**G** and **H**) Quantification of PDGFRα$^+$ (**G**) and GFAP$^+$ (**H**) vessels (*N* = 3). Representative images of maximum intensity projections (**A** and **F**) and single plane images (**E**) from vehicle and imatinib pretreated mice. Data points represent individual animals, bars the group mean ± SEM (**C**, **G** and **H**) and in **B** data points represent the group mean ± SEM. The dashed lines in **B**, **D**, **G** and **H** shows the pre-ischemia/contralateral group mean; hpi/dpi, hours/days post ischemia. Mixed-effects analysis with Tukey's post-hoc test (**B**); One-way ANOVA with Welch's test (**C**); Two-tailed, unpaired t-test with Welch's correction (**D**, **G** and **H**). *, # $P < 0.05$; ** $P < 0.01$; *** $P < 0.001$. Scale bars: 100 µm (**A**); 500 µm (**E**); 25 µm (**F**).

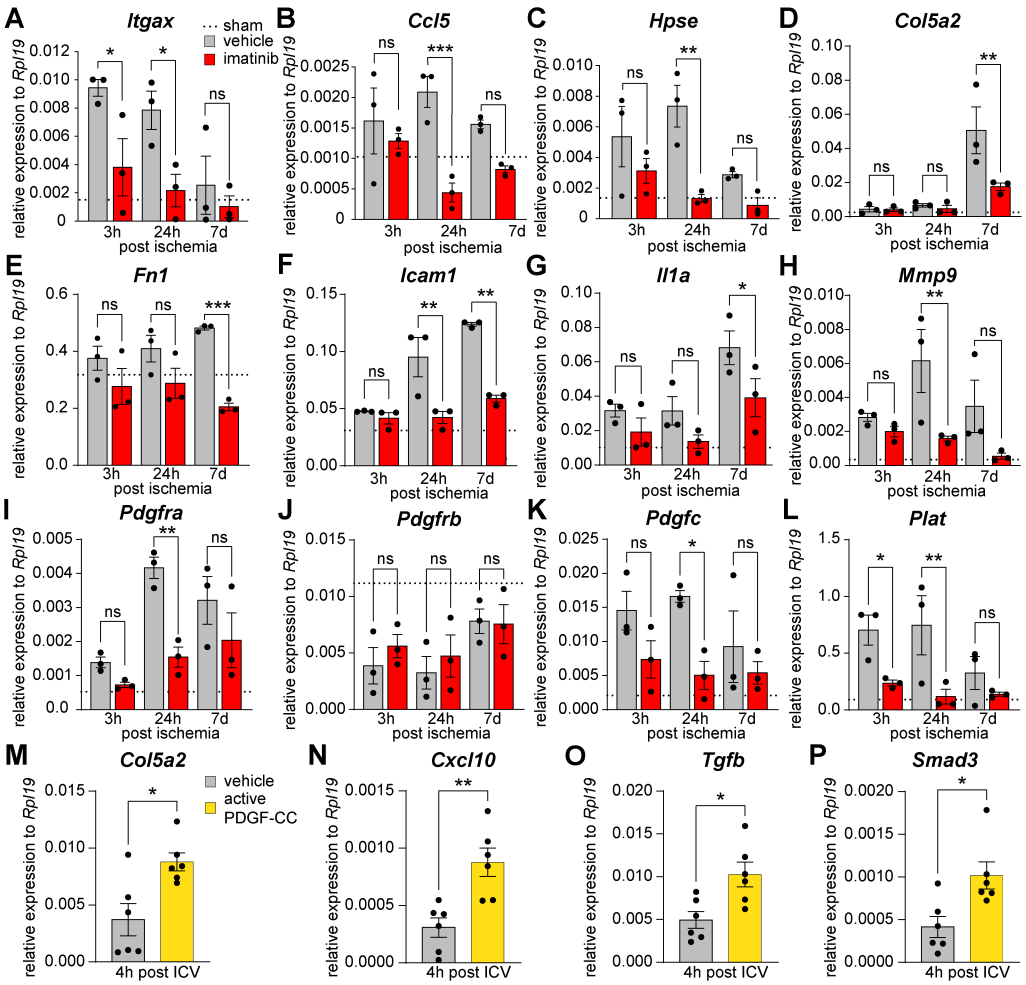

Figure 2. Imatinib dampens MCAO-induced, and PDGF-CC provokes, expression of pro-fibrotic/ pro-inflammatory genes in the cerebrovasculature. Gene expression analysis on RNA isolated from cerebrovascular fragments collected from the ipsilateral hemisphere of vehicle and imatinib pretreated mice at different time points after MCAO (**A-L**) or four hours after intracerebroventricular (ICV) injection with active PDGF-CC protein in naïve mice (**M-P**). (**A-L**) qPCR analysis of differentially expressed genes in the ischemic cerebrovasculature of vehicle and imatinib pretreated mice (*N* = 3). (**M-P**) qPCR analysis of expression of common fibrotic genes in cerebrovascular fragments isolated from wild-type mice 4 h after ICV injection of either vehicle or active PDGF-CC protein (*N* = 6). Data points represent individual animals, dashed lines show the sham-operated group mean. Two-way ANOVA with uncorrected Fisher's LSD (**A-L**); Two-tailed, unpaired t-test with Welch's correction (**M-P**). ns, non-significant; * $P < 0.05$; ** $P < 0.01$; *** $P < 0.001$.

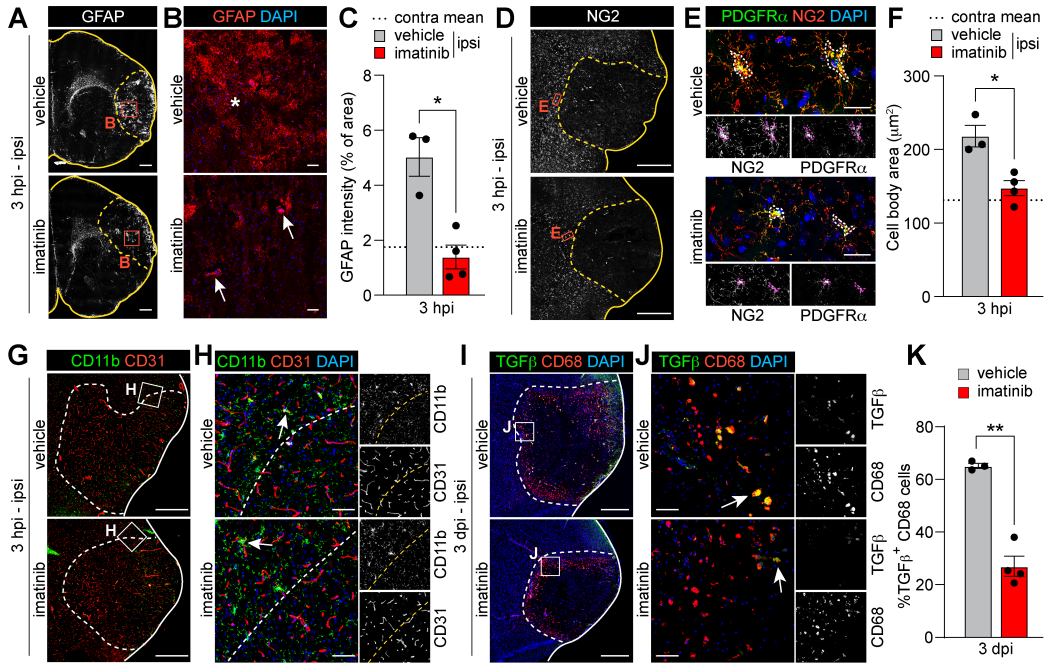

Figure 3. Imatinib attenuates the reactive gliosis response after MCAO. (**A** and **B**) Ipsilateral overviews (**A**) and high-magnifications from the ischemic area (**B**) of stainings for GFAP. Asterisk, non-perivascular GFAP signal. Arrows, perivascular GFAP signal. (**C**) Quantification of GFAP expression based on antibody immunoreactivity intensity above a set threshold (*N* = 3-4). (**D** and **E**) Ipsilateral overviews (**D**) and high-magnifications from the ischemic border (**E**) of co-stainings for NG2 and PDGFRα. Double positive cell-bodies encircled in **E**. (**F**) Quantification of PDGFRα⁺;NG2⁺-glia cell size in the peri-ischemic area (encircled in **E**) (*N* = 3-4). (**G** and **H**) Ipsilateral overviews (**G**) and high-magnifications from the ischemic border (**H**) of stainings for CD11b. Vessels visualized with CD31. Arrows, condensed CD11b⁺ microglia/infiltrating macrophages. (**I** and **J**) Ipsilateral overviews (**I**) and high-magnifications from the ischemic border (**J**) of co-stainings for CD68 and TGFβ. (**K**) Quantification of TGFβ expressing CD68⁺ microglia/infiltrating macrophages (arrows in **J**) in the ischemic area (*N* = 3-4). Representative images of immunofluorescent stainings and quantifications in brain sections from vehicle and imatinib pretreated mice collected at 3 hpi (**A-H**) or 3 dpi (**I-K**). Stitched epifluorescent images (**A**), single plane confocal images (**B**, **G** and **I**) and maximum intensity projections of confocal z-stacks (**D**, **E**, **H** and **J**). Ischemic area outlined with dashed lines. Data points represent individual animals, bars the group mean ± SEM and the dashed line the contralateral group mean. Hpi/dpi, hours/days post ischemia. Two-tailed, unpaired t-test with Welch's correction (**C**, **F** and **K**). * $P < 0.05$; ** $P < 0.01$. Scale bars: 500 µm (**A**, **D**, **G** and **I**); 50 µm (**B**, **H** and **J**); 25 µm (**E**).

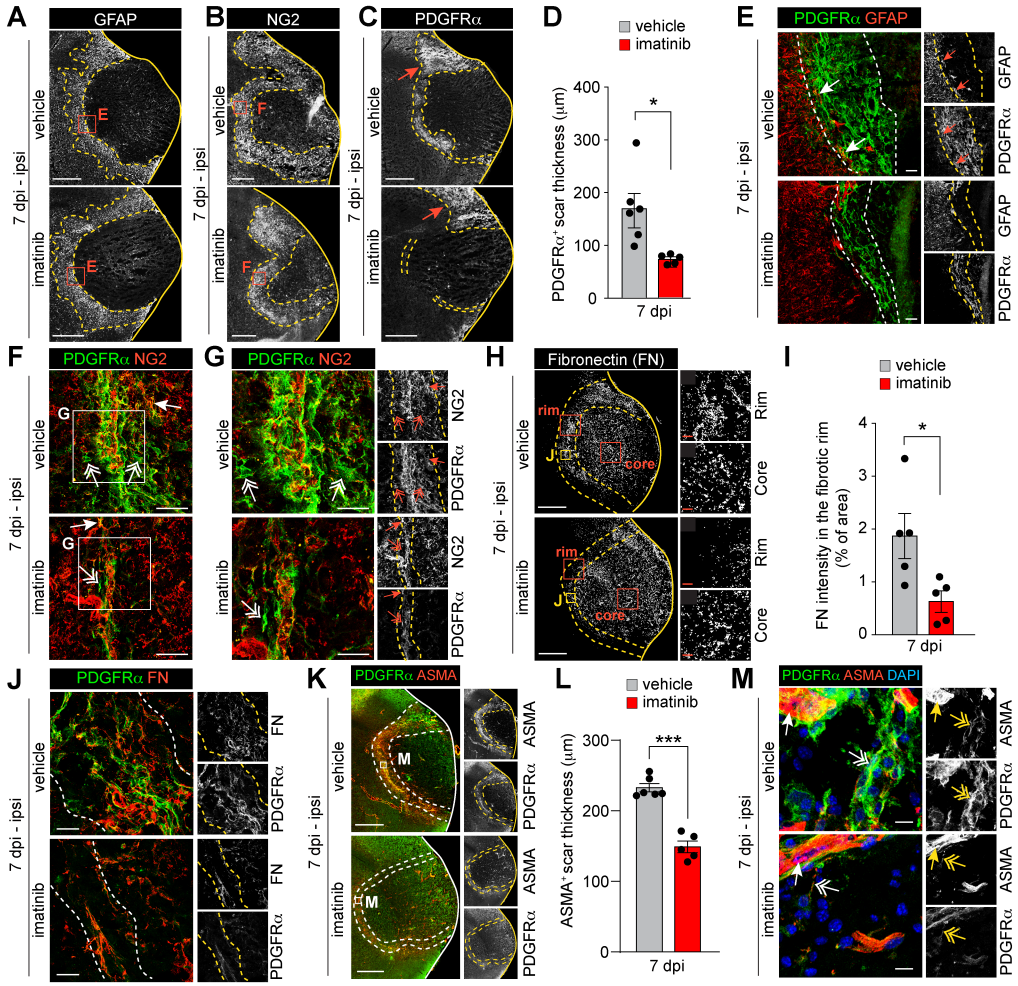

Figure 4. Imatinib specifically targets expansion of a PDGFRα⁺ myofibroblast scar in the fibrotic rim after MCAO. Representative images of immunofluorescent stainings and quantifications in brain sections from vehicle and imatinib pretreated mice collected at 7 days post ischemia (dpi). (**A-C**) Ipsilateral overviews from stainings for GFAP (**A**), NG2 (**B**) and PDGFRα (**C**). Arrows in **C**, PDGFRα⁺ scar not targeted by imatinib. (**D**) Quantification of PDGFRα⁺ scar thickness in the fibrotic rim (demarcated in **C**) (*N* = 5-6). (**E**) High-magnifications from the fibrotic rim from co-stainings for PDGFRα and GFAP. Arrows, PDGFRα⁺;GFAP⁺ cells. (**F** and **G**) Co-stainings for PDGFRα and NG2 acquired within the NG2⁺ glial scar. Arrows, PDGFRα⁺;NG2⁺ cells; two-headed arrows, non-perivascular PDGFRα⁺;NG2⁻ cells. (**H**) Ipsilateral overview and magnifications of the fibrotic rim and core from stainings for fibronectin (FN). (**I**) Quantification of FN expression in the fibrotic rim (demarcated in **H**) (*N* = 5). (**J**) High-magnifications from the fibrotic rim of co-stainings for PDGFRα and fibronectin. (**K**) Ipsilateral overviews from stainings for ASMA and PDGFRα. (**L**) Quantification of ASMA⁺ scar thickness in the fibrotic rim (demarcated in **K**) (*N* = 5-6). (**M**) High-magnifications from the fibrotic rim of co-stainings for ASMA and PDGFRα. Two-headed arrows, PDGFRα⁺;ASMA⁺ non-vascular cells; Arrows, ASMA⁺ vSMCs. Stitched epifluorescent images (**A-C** and **K**), single plane confocal images (**E** and **H**) and maximum intensity projections of confocal z-stacks (**F**, **G**, **J** and **M**). Dashed lines demarcate glia scar (**A** and **B**) and myofibroblast scar (**C-K**). Data points represent individual animals, bars the group mean ± SEM. Two-tailed, unpaired t-test with Welch's correction (**D**, **I** and **L**). * $P < 0.05$; *** $P < 0.001$. Scale bars: 500 µm (**A-C**, **H** and **K**); 50 µm (**E**, **F**, core/rim in **H**); 25 µm (**G** and **J**); 10 µm (**M**).

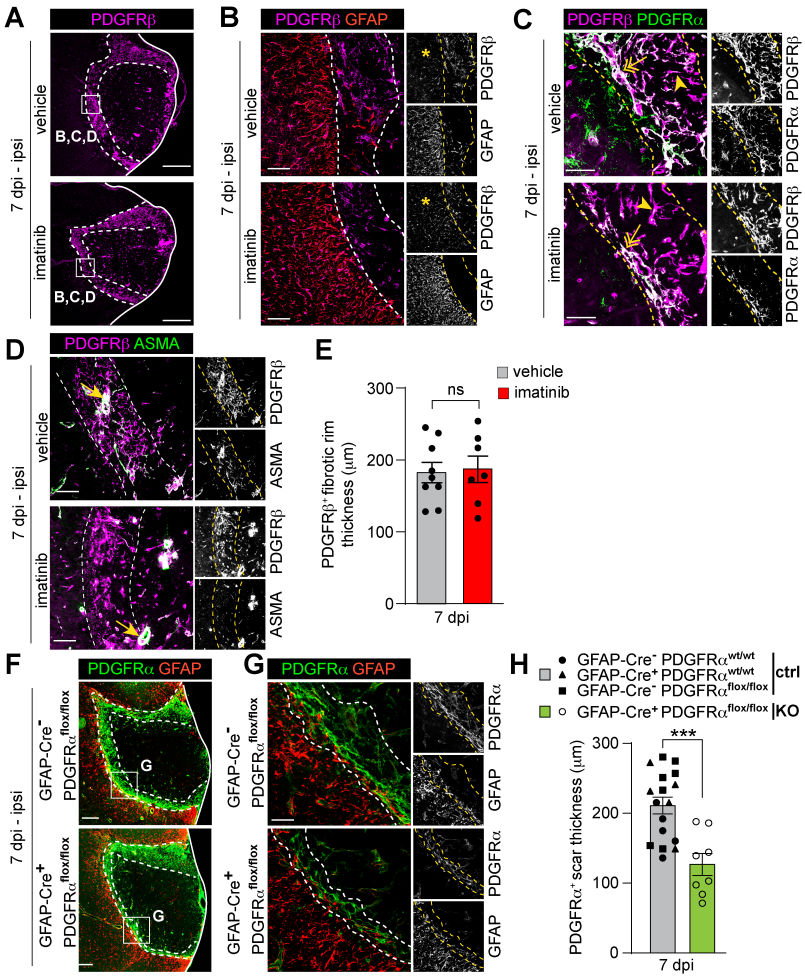

Figure 5. PDGFRα signaling drives expansion of the myofibroblast scar after MCAO. (**A-E**)and GFAP-Cre;PDGFRα flox mice (**F-H**) days post ischemia (). (**A**) Ipsilateral overview from stainings for PDGFRβ. (**B**) High-magnifications from the fibrotic rim of co-stainings for PDGFRβ and GFAP. Asterisks, PDGFRβ expression within the astroglia scar. (**C**) High-magnifications from the fibrotic rim of PDGFRα and PDGFRβ co-stainings. Two-headed arrows, PDGFRα^{high};PDGFRβ^{high} cells. Arrowheads, PDGFRα^{low};PDGFRβ^{high} cells. (**D**) High-magnifications from the fibrotic rim of co-stainings for PDGFRβ and ASMA. Arrows, ASMA^{+};PDGFRβ^{+} vSMCs. (**E**) Quantification of PDGFRβ^{+} scar thickness in the fibrotic rim (demarcated in A) (*N* = 7-9). Ipsilateral overviews (**F**) and high-magnifications from the fibrotic rim (**G**) of stainings for PDGFRα and GFAP in GFAP-Cre;PDGFRα flox mice. (**H**) Quantification of PDGFRα^{+} scar thickness in the fibrotic rim (demarcated in **F**). (*N* = 17 controls (ctrl), 8 PDGFRα-knockouts (KO)). Single plane (**A**) and maximum intensity projections of (**B-D** and **G**) confocal images, and stitched epifluorescent tiles (**F**). Dashed lines demarcate the PDGFRβ^{+} dense scar (**A-D**) and the myofibroblast scar (**F** and **G**) in the fibrotic rim. Data points represent individual animals and bars the group mean ± SEM. Two-tailed, unpaired t-test with Welch's correction (**E** and **H**). ns, non-significant; *** $P < 0.001$. Scale bars: 500 µm (**A** and **F**); 100 µm (**B** and **D**); 50 µm (**C** and **G**).

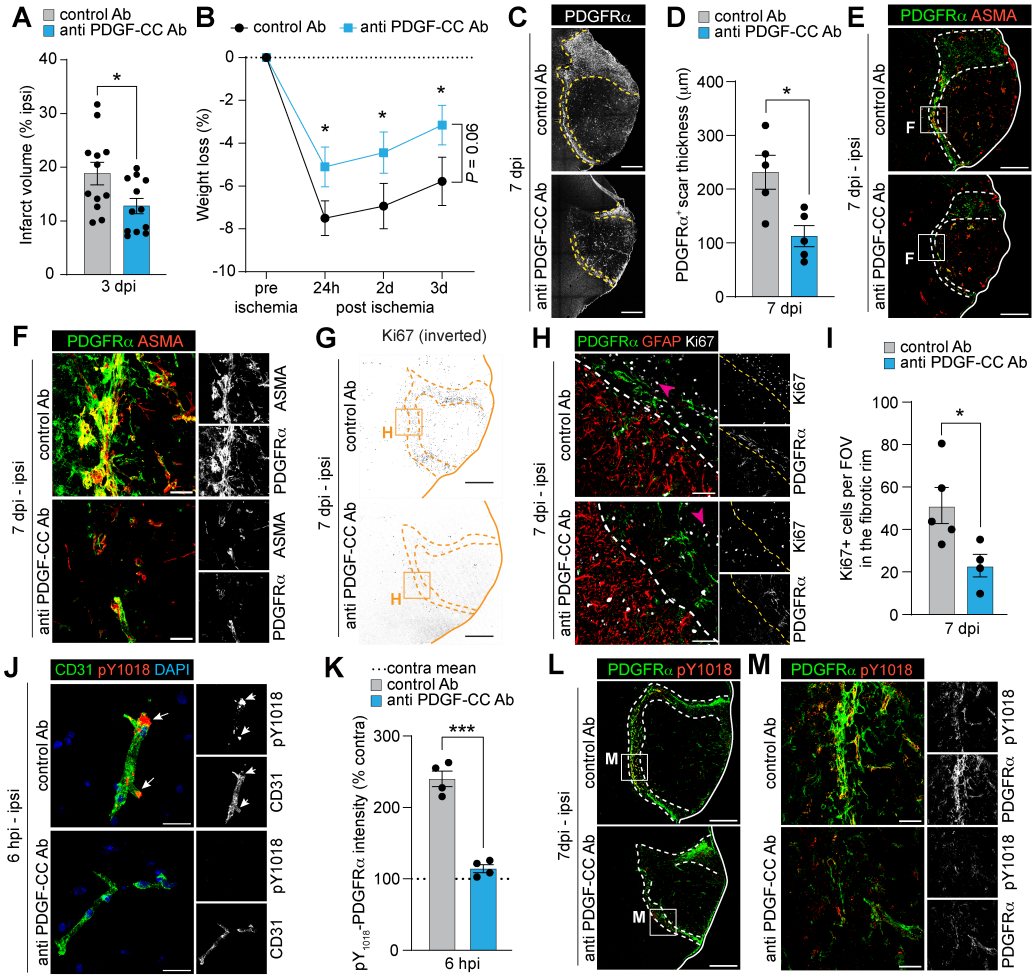

Figure 6. Anti-PDGF-CC antibody treatment reduces infarct volume and myofibroblast expansion in the fibrotic rim after MCAO. (**A**) Infarct volume 3 days post ischemia (dpi) (*N* = 12). (**B**) Weight during the first 3 dpi (*N* = 12). (**C-M**) Representative images of immunofluorescent stainings and quantifications in brain sections from control and anti-PDGF-CC antibody pretreated mice collected at 6 hours post ischemia (hpi) to 7 dpi. (**C**) Ipsilateral overviews of PDGFRα stainings at 7dpi. (**D**) Quantification of PDGFRα$^+$ scar thickness in the fibrotic rim (demarcated in **C**) (*N* = 5). (**E-H**) Co-stainings of PDGFRα and ASMA (**E** and **F**) and PDGFRα, GFAP and Ki67 (**G** and **H**) at 7 dpi. Arrowheads, proliferating PDGFRα$^-$ cells. (**I**) Quantification of Ki67$^+$ nuclei in the fibrotic rim (*N* = 4-5). (**J**) High-magnifications from the ischemic area at 6 hpi of stainings for phospho-PDGFRα (pY1018) and CD31. Arrows, phosphorylation of perivascular PDGFRα. (**K**) Quantification of perivascular phospho-PDGFRα expression in the ischemic area at 6 hpi (*N* = 4). (**L** and **M**) Co-stainings for phospho-PDGFRα (pY1018) and total PDGFRα at 7dpi. Stitched epifluorescent tiles (**C**) and single plane (**E**, **G** and **L**)/maximum intensity projections (**F**, **H**, **J** and **M**) of confocal images. Dashed lines demarcate the myofibroblast scar (**C**, **E**, **G** and **L**) and the glia border (**H**). Data points represent individual animals and bars the group mean ± SEM (**A**, **D**, **I** and **K**), in **B** data points represent the group mean ± SEM. Dashed line in **K** shows contralateral group mean. Two-tailed, unpaired t-test with Welch's correction (**A**, **D**, **I** and **K**); Two-way repeated measures ANOVA with Tukey's post-hoc test (**B**). ns, non-significant; * $P < 0.05$; ** $P < 0.01$, *** $P < 0.001$. Scale bars: 500 µm (**C**, **E**, **G** and **L**); 50 µm (**F**, **H** and **M**); 20 µm (**J**).

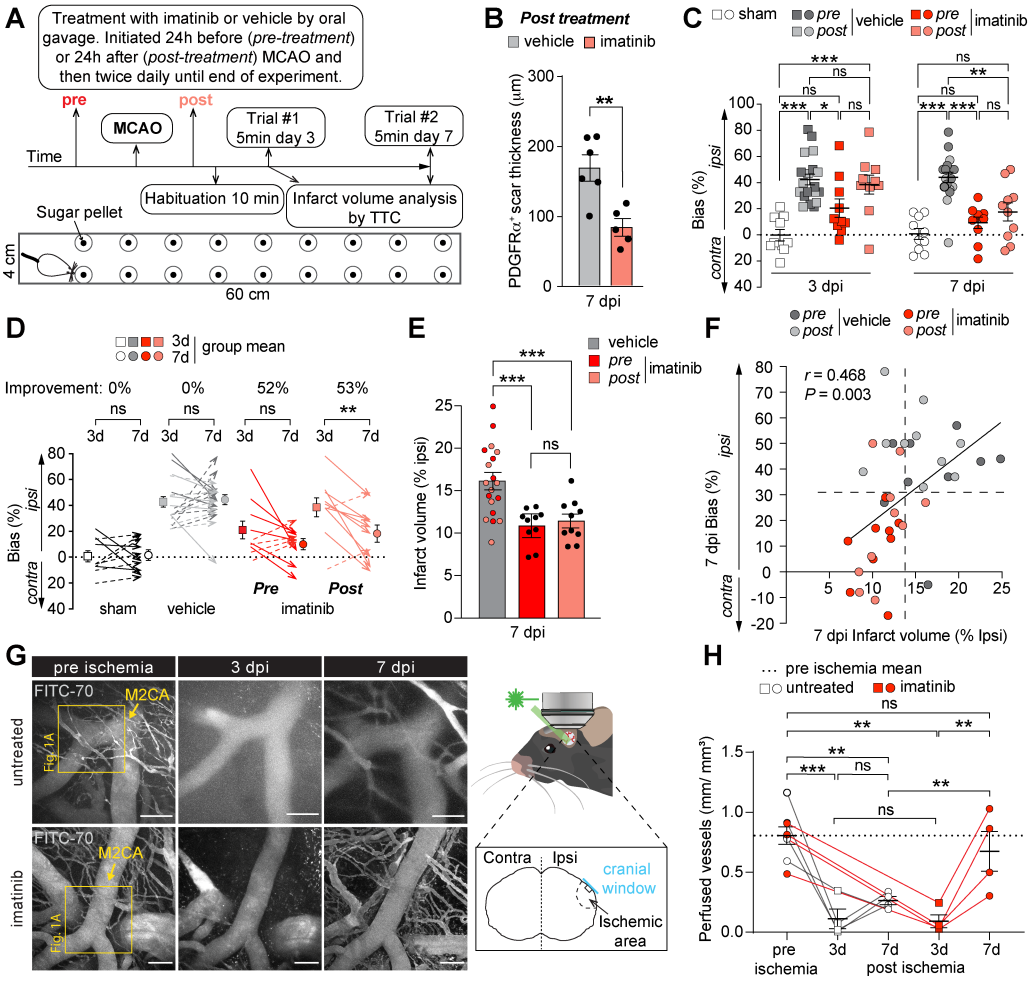

Figure 7. Imatinib progressively improves functional recovery after MCAO. (**A**) Schematic illustration of experimental design and the corridor task. The number of pellet explorations made from the left (ipsilateral to the lesion) or right (contralateral) side were counted. (**B**) Quantification of PDGFRα^{+} scar thickness in the fibrotic rim in imatinib post-treated mice at 7 days post ischemia (dpi) (*N* = 5-6). (**C**) Exploration bias in vehicle, imatinib pre- and post-treated as well as sham-operated mice (*N* = 10-19). (**D**) Change in exploration bias between 3 dpi and 7 dpi. Arrows, individual mice (*N* =10-19). (**E**) Infarct volume at 7 dpi of vehicle and pre- or post-treated mice (*N* = 10-19). (**F**) Correlation of infarct volume with exploration bias at 7 dpi (*N* = 9-10). (**G**) Representative maximum intensity two-photon images of FITC70 signal before ischemia (pre) and at different time points after (post). (**H**) Quantification of vascular perfusion as assessed by intraluminal FITC70 signal utilizing longitudinal two-photon microscopy (*N* = 4). Data points represent individual animals and bars the group mean ± SEM (**B**, **C**, **E**, **F**, **H** and **I**), in **D** arrows represent individual animals and data points represent the group mean ± SEM. Two-tailed, unpaired t-test with Welch's correction (**B**); Two-way repeated measures ANOVA with Tukey's post-hoc test (**C**, **D** and **H**); One-way ANOVA with Welch's test (**E**); Linear Regression (**F**). ns, non-significant; * $P < 0.05$; ** $P < 0.01$; *** $P < 0.001$. Scale bars: 500 µm (**B**); 100 µm (**G**).